Int. J. Electrochem. Sci., 11 **(2016)** 9959 – 9971, doi: 10.20964/2016.12.69

International Journal of ELECTROCHEMICAL SCIENCE
www.electrochemsci.org

Biosynthesis of Silver Nanoparticles using *Mimosa Pudica* Plant root extract: Characterization, Antibacterial Activity and Electrochemical Detection of Dopamine

V. Sreenivasulu[1], *N. Siva Kumar*[2,*], *M. Suguna*[3], *M. Asif* [2,*], *Ebrahim H. Al-Ghurabi*[2], *Z. X. Huang*[1], *Z. Zhen*[1]

[1] Institute of Atmospheric Environmental Safety and Pollution Control, Jinan University, Huangpu Road West 601, Guangzhou 510632, China
[2] Department of Chemical Engineering, King Saud University, P.O. Box 800, Riyadh 11421, Saudi Arabia
[3] Biopolymers and Thermo physical Laboratories, Department of Chemistry, Sri Venkateswara University, Tirupati – 517502, A.P., India.
[*]E-mail: shivanadavala@gmail.com, snadavala@ksu.edu.sa, masif@ksu.edu.sa

Received: 24 August 2016 / *Accepted:* 13 October 2016 / *Published:* 10 November 2016

In this paper, we report an environmentally friendly, fast and cost-effective method for the synthesis of silver nanoparticles using aqueous *Mimosa pudica* root extract as reducing and stabilizing agent. Synthesized silver nanoparticles were confirmed by analyzing the excitation of surface plasmon resonance (SPR) using UV-visible spectrophotometer peak at 430 nm. The presence of functional groups in the plant extracts were identified by FTIR analysis. Spherical shaped, crystalline in nature and 35-42.5 nm sized particles were recorded using TEM and XRD analysis. The surface morphology of the AgNPs was identified by using SEM while the energy-dispersive X-ray spectroscopy (EDAX) confirmed the presence of silver metal ion. The aqueous root extract of *M. pudica* exhibited significant antimicrobial activity against both gram positive (B. subtilis) and gram negative (E. coli, P. aeruginosa) microorganisms. Moreover, Cyclic Voltammetry (CV) results showed a substantial enhancement of peak current using synthesized AgNPs-assembled-glassy carbon electrode (GCE) as compared to bare-GCE. The present AgNPs-assembled-GCE displayed very high sensitivity and excellent linearity to the detection of dopamine (DA) which is a neurotransmitter released by the brain.

Keywords: Biosynthesis; Mimosa pudica root extract; Silver nanoparticles; Antibacterial activity; Dopamine; Cyclic Voltammetry.

1. INTRODUCTION

Metallic nanoparticles have become the focus of intensive research owing to their unique properties, and are therefore gaining an ever-increasing application in diverse areas such as drug

delivery, catalysis, environmental protection and energy conversion [1–5]. Metallic nanoparticles are currently synthesized using various methods such as physical vapor deposition, chemical vapor deposition, sol gel method, electro-chemical synthesis, microwave assisted synthesis, plasma polymerization, laser ablation, emulsion polymerization, laser CVD and pyrolysis [6]. However, these methods are non-eco-friendly since they often require large amounts of toxic chemicals and high temperature processing conditions. Therefore, researchers are increasingly turning to biological systems for nanoparticle synthesis [7–8]. As an eco-friendly alternative to various physical and chemical processing technique for the synthesis metallic nano-particles, the use of microorganisms, enzyme, fungi, algae and plant extract haves been suggested [9–13].

Recent literature survey suggests that plants or plant extracts, which act as reducing and capping agents for nanoparticles synthesis, are faster, reliable and cost-effective over other biological processes [14–15]. Several studies have reported the synthesis of AgNPs using different parts of plant materials such as leaf extracts of Solanum indicum [16], Azadirachta indica [17], Croton sparsiflorus morong [18], Skimmia laureola [19], Mimosa pudica leaves [20], fruit extracts [21–22], bark extract [23], fruit peel extract [24] and root extracts [25–28].

Mimosa pudica *(Family: Fabaceae / Mimosaceae) also called* sensitive plant or shy plant, which are known as Touch me not in English, Chhui-mui in Hindi, and Attapatti in local Telugu language. This is an important and *highly valuable ayurvedic medicinal plant, which is easily available* throughout India. *Its* roots contain tannin, ash, calcium oxalate crystals and alkaloid mimosine, and therefore suggested for the treatment of skin diseases, high blood pressure, diarrhoea, amoebic dysentery, and gynaecological disorders etc.

In the present work, we first investigated the facile and stable biosynthesis of silver nanoparticles (AgNPs) from aqueous root extract of *M. pudica.* The formation of AgNPs were identified using UV–visible spectrophotometer. The synthesized AgNPs were thoroughly characterized by using XRD, FTIR, SEM, EDAX and TEM, and their antibacterial activities against some selected bacterial strains were also examined. Next, we investigated the electrochemical responses of both bare-GCE and AgNPs-assembled-GCE using Cyclic Voltammetry to delineate the performance enhancement due to AgNPs. Finally, sensitivity of the AgNPs-assembled-GCE to DA concentration was investigated by using differential pulse voltammetry technique (DPV).

2. EXPERIMENTAL METHODS

2.1. Materials

High purity analytical grade chemical and reagents were used in the present study. Silver nitrate ($AgNO_3$) was obtained from Merck (Mumbai, India). Dopamine hydrochloride, sodium dihydrogen ortho phosphate (NaH_2PO_4), and disodium hydrogen phosphate (Na_2HPO_4) from obtained from Hi Media Laboratories, Mumbai, India. A dopamine stock solution (25 mM) was prepared by adding dopamine to 0.1 M perchloric acid. Phosphate buffer solution was prepared by adjusting the pH with 0.2 M NaH_2PO_4 and Na_2HPO_4 solution. All the aqueous solutions were prepared by using double distilled water. All glassware were washed in dilute HNO_3 and hot dried in oven. The *M. pudica* roots

were collected from local area of Sri Venkateswara University campus, Chittoor district, Andhra Pradesh, India.

2.2. Preparation of M. pudica root extract

The *M. pudica* plant roots were washed several times with tap water and distilled water to remove dust and other contaminants, then cut into fine pieces, and dried under shade at room temperature. 30 g roots were added to 100 ml ultrapure water in 250 ml Erlenmeyer flask, heated in water bath at 50 °C for 30 min. The mixture was then cooled to room temperature and filtered using Whatman Grade 1 in order to obtain the aqueous root extract. The product thus obtained was stored at 4 °C for further analysis.

2.3. Synthesis of Ag nanoparticles (AgNPs)

We first prepare 1 mM silver nitrate ($AgNO_3$) solution. In order to prevent oxidation, the solution was stored in an amber-colored bottle. To synthesize silver nanoparticles, 10 mL of the *M. pudica* fresh aqueous root extract was added into 90 ml of 1 mM silver nitrate solution, and the mixture continuously stirred for about 10-15 min. The solution was then incubated for 1 h at the room temperature. The colour of the resulting mixture was found to change from pale yellow to dark brown indicating the formation of silver nanoparticles (AgNPs) by *M. pudica* root extract. The resultant solution containing the AgNPs was centrifuged at 4000 rpm for 10 minutes. The collected sample AgNPs were allowed to dry in a watch glass then stored for further characterization studies.

2.4. Characterization of AgNPs

The detailed morphology of synthesized AgNPs was investigated using Transmission Electron Microscopy (Model: Hitachi H-700, Japan) with an acceleration voltage of 120 kV at room temperature. The surface morphology was also studied using Scanning Electron Microscopy (Model Evo15, CarlZeiss, England). The configuration of AgNPs was determined by XRD, Powder X-ray diffraction patterns were recorded on a Bruker D8-Advance diffractometer using graphite monochromatic CuKα1 (1.5406 Å) and Kα2 (1.5439 Å) radiations. In order to confirm the synthesis of AgNPs, UV-visible spectra, in the range of 200–800 nm, were recorded as a function of the reaction time using spectrophotometer (Shimadzu, Japan). The sample composition and elemental contents were analyzed by using energy dispersive analysis system of X-ray (EDAX). Fourier Transform infrared (FTIR) spectra of the samples were recorded with the help of FTIR (Thermo-Nicolet IR- 200 series model, Germany) in the range of 4000-400 cm^{-1} using KBr pellets in order to determine the possible functional groups involved in the formation of nanoparticles. Antibacterial activities of the biosynthesized AgNPs were carried out on the E.coli, Bacillus subtilis and Pseudomonas aeruginosa using the standard disk diffusion method. Using Streptomycin antibiotic, the zone of inhibition (ZI) was determined during the sensitivity analysis. For electrochemical studies, Autolab PG STAT101

(Metrohm Autolab B.V., Netherlands) was employed. The electrode configuration consists of three electrodes; glassy carbon electrode (GCE) as a working electrode, saturated Ag/AgCl/KCl as a reference electrode whilst Pt wire acts as a counter electrode. AgNPs-assembled-GCE was prepared by drop casting method. For the measurement of the pH of the buffer solution, an Elico LI-120 pH meter (Elico Ltd, India) was used.

3. RESULTS AND DISCUSSION

3.1. UV-Visible Spectroscopy analysis

Our objective is the eco-friendly green synthesis of AgNPs using the *M. pudica* root extract. Its addition to the silver nitrate solution causes the change of the color of the reaction mixture from pale yellow to dark brown owing to the excitation of surface plasmon resonance (SPR) by AgNPs. Figure 1 shows UV-Vis Spectra at different reaction times. The sample exhibits an absorbance band at about 430 nm wavelength. As the reaction time increases, the absorbance peaks become sharper as shown in Figure 1(a) to (d). The increase in the intensity of peak could be due to increase in the number of Ag nanoparticles in the reaction medium. After reaching a particular intervals of time (i.e 60 minutes duration), the absorbance peak of Ag nanoparticles increases very slowly (nearly constant) as shown in the Figure 1(d). This is due to the reduction of all the Ag ions present in the reaction medium into Ag nanoparticles. In our experiments, the optimal reaction was found to be 60 minutes.

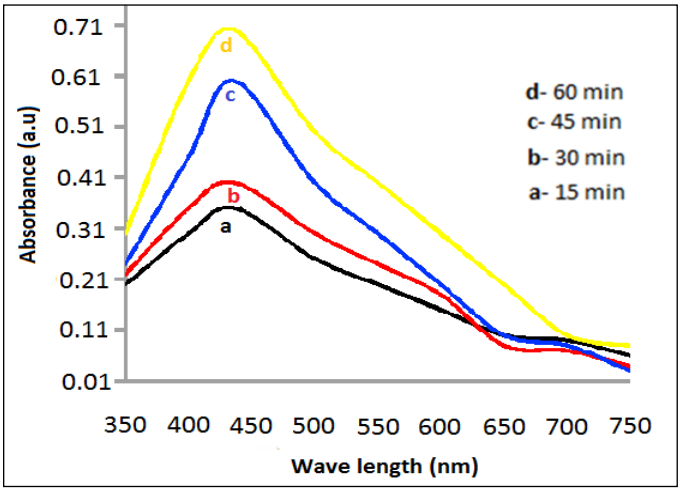

Figure 1. UV-visible absorption Spectra of AgNPs synthesized by aqueous root extract of M. pudica at different recation times.

3.2. FTIR analysis of AgNPs

The FTIR spectrum was used for the identification of functional groups that caused the reduction of silver ions and capping of the bio-reduced AgNPs. The corresponding transmittance peaks at 3314.24, 2128.46, 1636.26 and 583.23 cm^{-1} for synthesized AgNPs are shown in Figure 2. Strong

absorption broad band peak observed at 3314.24 cm^{-1} corresponds to primary amine (–NH) or hydroxyl (–OH) groups [29]. On the other hand, the 1636.26 cm^{-1} band can be associated with the stretching vibration of carbonyl group (–C=O) [30]. The formation of AgNPs in the reaction mixture was reflected in the broadening of the peak corresponding to the amide I band at 1636.26 cm-^{1}, which indicated the capping of the AgNPs by proteins. The FTIR spectra thus confirms that different functional groups, i.e. –C=O (Carbonyl), –OH (hydroxyl) and C-N (amine) actively participates in the biosynthesis of AgNPs [31].

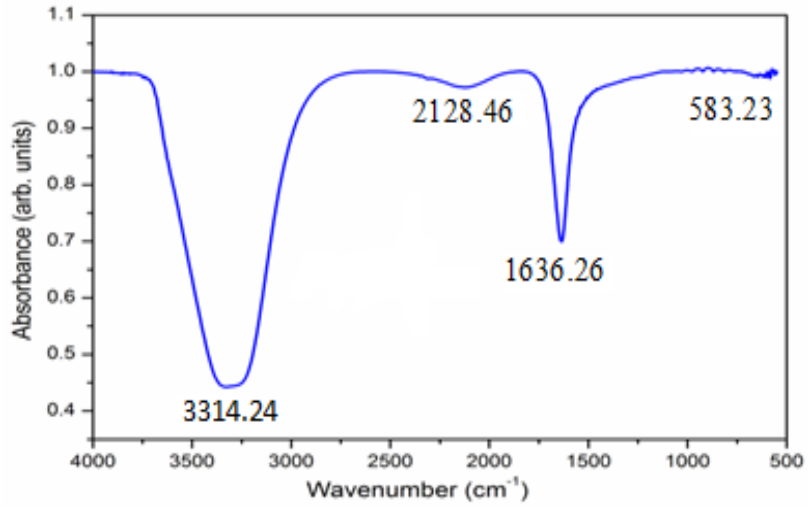

Figure 2. FTIR spectrum of synthesized AgNPs using aqueous root extract of M. pudica.

3.3. TEM analysis of AgNPs

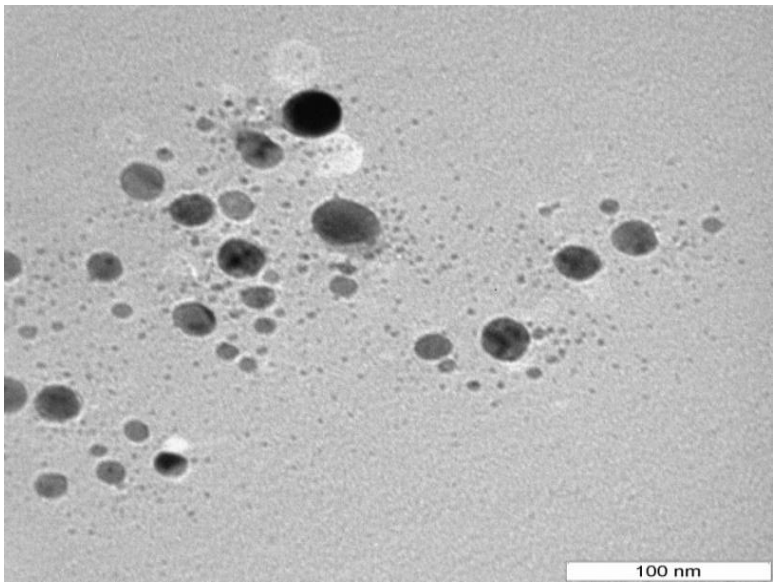

Figure 3. TEM micrograph of synthesized AgNPs using aqueous root extract of M. pudica.

Owing to extremely high resolution of transmission electron microscopy (TEM), it can be used to obtain necessary information about the size and morphology of the synthesized nanoparticle [32]. Figure 3 shows TEM micrograph of AgNPs. The crystallite in our samples were found to be well isolated and nearly spherical in shape. The average particle diameter is approximately 35 nm that is close to the aggregate sizes observed by TEM.

3.4. SEM and EDAX analysis of AgNPs

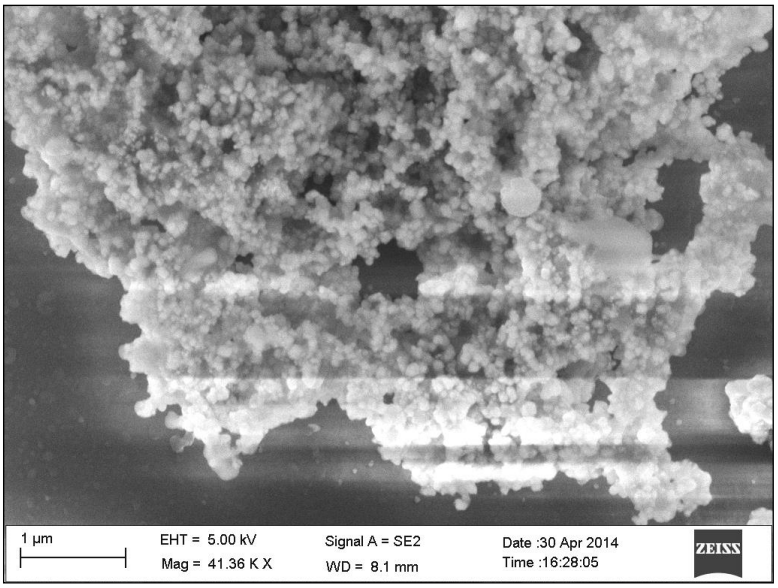

Figure 4. SEM micrograph of synthesized AgNPs using aqueous root extract of M. pudica.

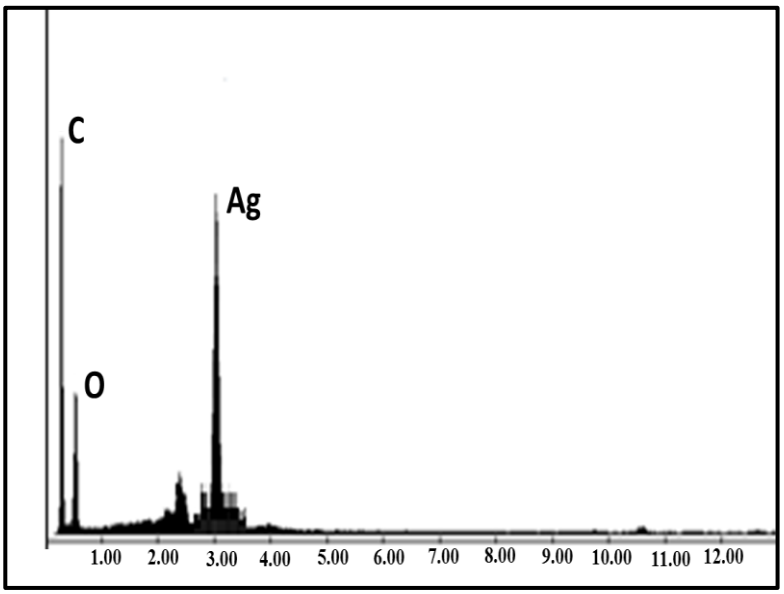

Figure 5. EDAX spectra of synthesized silver nanoparticles.

Scanning electron microscopy represents a powerful tool for the morphological characterization of synthesized nanomaterials with a high degree of spatial resolution. Figure 4 shows

the SEM image of the synthesized silver nanoparticles sample. One can clearly see the formation of agglomerates of spherical bead like structure of AgNPs with a uniform size distribution. As seen in Figure 5, the Energy Dispersive X-ray analysis (EDAX) graph confirms the presence of elemental silver. Metallic silver nanocrystals generally exhibit typical optical absorption peak at 3 keV due to their surface plasmon resonance [33]. Furthermore, the other peaks carbon and oxygen atoms are also suggested the presence of organic moieties on the surface of silver nanoparticles which might have come from the plant root extract.

3.5. XRD analysis of AgNPs

The XRD results of the synthesized silver nanoparticles are shown in Figure 6. The XRD spectrum shows four distinct diffraction peaks at 2θ = 38.28°, 44.33°, 64.33° and 78.53° corresponding lattice plane value was indexed to the (111), (200), (220) and (311) planes of pure metallic silver, confirming the formation of AgNPs. All the diffraction peaks are well indexed to the Face Centered Cubic (FCC) structure (JCPDS file number: 00-004-0783). We did not notice any diffraction peaks in the XRD pattern that might suggest the presence of impurities in our AgNPs sample, thereby confirming the high purity of the synthesized product. The intensity of the peak increases at (111) plane, indicating increased crystallinity. The average grain crystalline size of green synthesized AgNPs was calculated by using Debye-Scherrer's formula [34],

$$D = \frac{K\lambda}{\beta cos\theta} \quad (1)$$

where D is the crystallite size (nm), λ is the wavelength of incident X-ray (nm), K is the dimensionless shape factor, β is the full width at half maximum (FWHM), and θ is the Bragg diffraction angle. The average crystallite size of the AgNPs is estimated to be around 42.5 nm by using Scherer's equation.

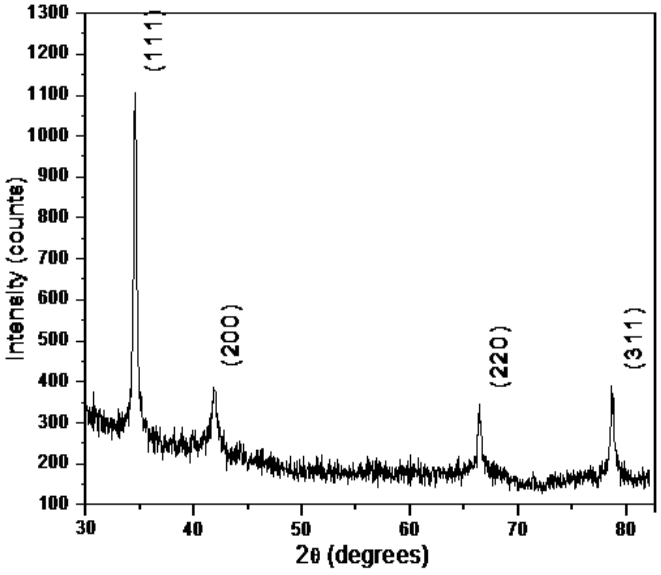

Figure 6. XRD patterns of synthesized AgNPs using aqueous root extract of M. pudica.

3.6. Antibacterial activity of AgNPs

The antimicrobial activity was determined by the disk diffusion method. The extracted silver nanoparticles tested for their antibacterial activity against laboratory test organisms like *Escherichia coli*, *Bacillus subtilis* and *Pseudomonas aeruginosa* as shown in Figure 7A–C, respectively. The solidified nutrient agar medium plates were inoculated with 100 µL of each bacterial culture and approximately 0.5 mm diameter disks were prepared placed on the surface of the inoculated agar medium plates. Different volumes of extracted AgNPs were loaded along with standard *Streptomycin* antibiotic for positive control and all the plates were incubated 37˚C for 24 hours. The exact mechanism of efficient antibacterial effect of AgNPs against various bacteria is not clearly understood. This may be attributed to the electrostatic attraction between the positively charged nanoparticles and the negatively charged cell membrane of micro-organism. Due to the electro-static attraction, metallic AgNPs attach to the surface of the cell membrane, thereby affecting its permeability and damaging cell respiration behavior. Since the binding of nanoparticles to the bacteria depends on the surface area available for interaction, smaller silver nanoparticles, owing to their larger surface area as compared to their larger counterpart, exhibit greater antibactericidal activity [35]. Another plausible mechanism attributed to bacterial cell death is the penetration of the bacterial cell wall by AgNPs, causing the deterioration in plasma membrane [36]. Our synthesized AgNPs showed higher antimicrobial activity against *E.coli* and *B. subtilis* as compared to *P. aeruginosa.*

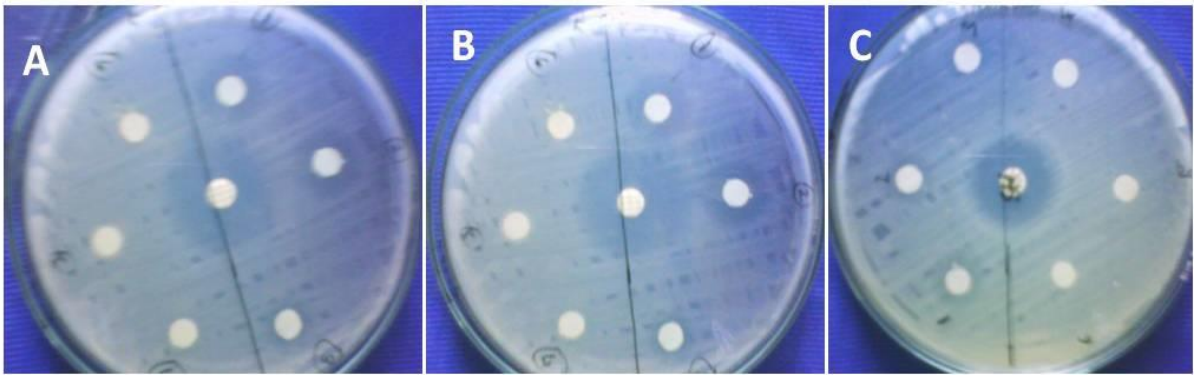

Figure 7. Antibacterial activity of aqueous root extract of M. Pudica: (A) Escherichia coli (B) Bacillus subtilis (C) Pseudomonas aeruginosa.

3.7. Electrochemical behavior of AgNPs

Electrochemical sensing activity of green synthesized AgNPs was measured by Cyclic Voltammetry (CV). Figure 8 shows the response of 1.5×10^{-5} M $[Fe(CN)_6]^{3-/4-}$ in a 10.0 µM HCl solution at the bare-GCE and AgNPs assembled electrodes at a scan rate of 100 mVs^{-1}. The electrochemical sensing activity of a redox couple in the solution on the AgNPs assembled electrodes depend on the surface of the GCE. Results exhibits low current signal for bare-GCE as shown in Figure 8a. However, the cyclic voltammetry response is clearly improved at AgNPs-assembled-GCE,

reflected by the enhancement of the peak currents (Ip) as shown in Figure 8b. This is due to the addition of silver colloidal nanoparticles on the bare-GCE. AgNPs has excellent conductivity and large specific surface area, which caused the AgNPs-assembled-GCE exhibit improved catalytic performance as compared with bare-GCE. Thus, the AgNPs-assembled-GCE demonstrated a relatively low oxidation potential, lower detection limit and high sensitivity than those recently reported elsewhere [37–41]. The AgNPs-assembled-GCE therefore can be used as preparation of electrochemical sensors for detection of dopamine, 4-(2-Aminoethyl) benzene-1,2-diol (DA) that plays several important roles in the brain and body.

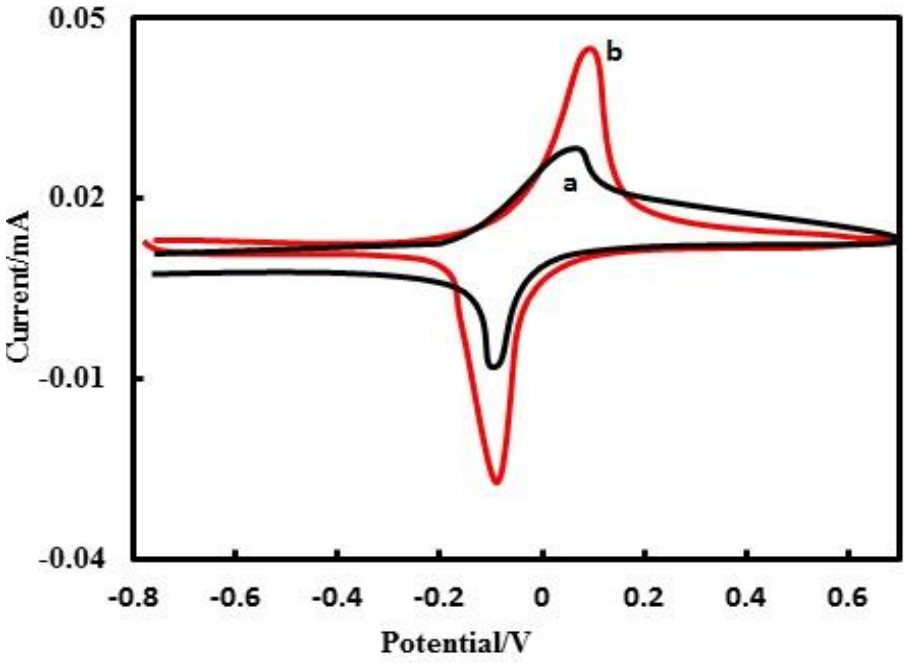

Figure 8. Typical 3D cyclic voltammograms for the bare-GCE (a) and AgNPs assembled-GCE (b) in the presence of 1.5×10^{-5} M $[Fe(CN)_6]^{3-/4-}$ in a 10.0 μM HCl solution at 100 mVs^{-1}.

3.8. Electrochemical response of dopamine (DA) at the bare-GCE and AgNPs/GCE

Figure 9 shows the electrochemical responses of 1×10^{-5} M DA in 0.2 M phosphate buffer solution of pH 7.0 at the bare-GCE and AgNPs-assembled-GCE at a scan rate 100 mVs^{-1}. Compared with the GCE, the remarkable enhancement in the peak currents with the reduction of over potential showed electro-catalytic effects of the Ag nanoparticles. This is mainly due to the high surface area of AgNPs-assembled-GCE that helps to increases the electro-catalytic activity of the electrode. In addition, the prepared AgNPs-assembled-GCE exhibits excellent electrochemical response for oxidation of dopamine, nearly twice as compared with GCE. This is probably due to the silver nanoparticles contributing to the immediate electronic conductivity and promoting the electron transfer rate of the electrode [42-45].

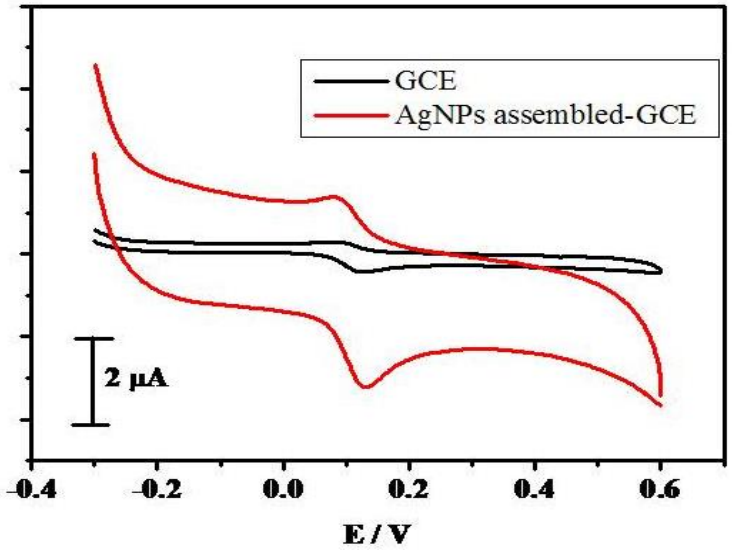

Figure 9. Cyclic voltammogram of 1×10^{-5} M DA in PBS at pH 7.0 at GCE and AgNPs-assembled-GCE.

3.9. Sensitivity Analysis

The differential pulse voltammetric technique (DPV) was carried out to determine sensitivity of the AgNPs-assembled-GCE prepared here to the DA concentration. As shown in Fig 10, the concentration was varied in the range of 10-60 μM and the corresponding variation of the peak anodic current (Ipa) was recorded. The graph shows a linear increase in Ipa with the increase in the DA concentration with a correlation coefficient (R^2) of 0.998. The detection limit of dopamine was 0.5 μM at AgNPs-assembled-GCE. In addition, these results (Table 1) are comparable with those previously reported in the literature [46-56].

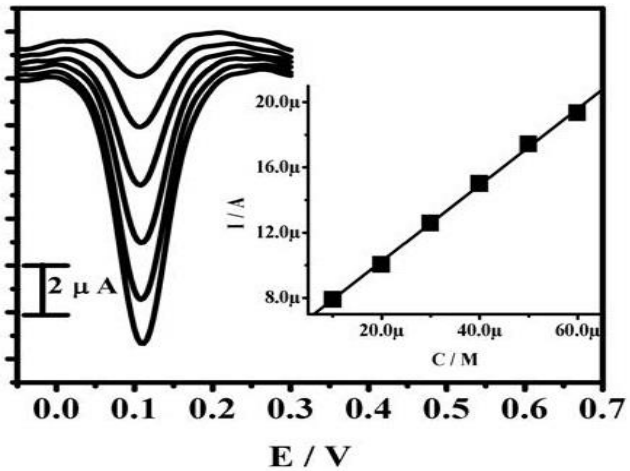

Figure 10. Differential pulse voltammogram of (a) 1.0×10^{-5} M, (b) 2×10^{-5} M, (c) 3×10^{-5} M, (d) 4×10^{-5} M , (e) 5×10^{-5} M, (f) 6×10^{-5} M DA in 0.2 M phosphate buffer solution of pH 7.0 at AgNPs-assembled-GCE.

Table 1. Comparison of analytical parameters of the present work and previously reported methods for determination of dopamine.

S.No	Electrode	Technique	pH	Linear range (μM)	Detection limit of Dopamine (μM)	References
1	Poly (vinyl alcohol) covalently modified-GCE	DPV	7.0	2.0-70	1.4	46
2	PTCA-Cys-AuNPs/GCE	CV	4.0	0.04-100	0.010	47
3	Activated-GCE	DPV	6.0	0.65-18	0.62	48
4	Ordered mesoporous carbon/Nafion composite film modified GCE	DPV	7.4	1.0-90	0.5	49
5	Poly(acid chrome blue K) modified GCE	DPV	4.0	1.0-200	0.5	50
6	Graphene modified electrode	DPV	7.4	4-100	2.64	51
7	CDDA/GCE	DPV	4.0	5.0-280	0.29	52
8	Graphene-doped film of layered double hydroxides modified GCE	CV	7.0	1.0-199	0.3	53
9	GCE/MWCNT-FeNAZ-CH	CV	1.0	7.35-833	1.05	54
10	Poly(indole-6-carboxylic acid) (PICA-TCNQ-GCE)	CV	7.4	0.001-0.1	4.0	55
11	F-MWCNT/GCE	DPV	8.0	3-200	0.8	56
12	Pdop@GR/MWCNTs/GCE	DPV	7.0	7.0-297	1.0	57
13	MP-GR/GCE	DPV	6.5	4.0-40	1.5	58
14	AgNPs/GCE	DPV	7.0	10-60	0.5	Present work

*Glassy carbon electrode (GCE), Cyclic Voltammetry (CV), Differential Pulse Voltammetry.

4. CONCLUSIONS

The proposed method is simple and green approach to synthesize silver nanoparticles (AgNPs) using the aqueous *Mimosa pudica* root extract. The characterization with FTIR and UV–Vis spectrophotometer is the preliminary evidence for the formation of silver nanoparticles. The purity and the crystallinity in nature and spherical in shape of the synthesized AgNPs were confirmed by XRD and TEM studies. The average grain particle sizes were in the range from 35 to 42.5 nm. SEM revealed that the AgNPs were spherical in shape and EDAX result confirmed the presence of silver along with other elements in the root extract. The AgNPs clearly showed higher antibacterial activity against *Escherichia coli* and *Bacillus subtilis* as compared to *Pseudomonas aeruginosa*. Moreover, CV results showed more than 100% increase in the the peak current using AgNPs-assembled-GCE as compared to bare-GCE. The enhanced sensitivity of the AgNPs-assembled-GCE helped to detect extremely low dopamine concentration with a high degree of linearity.

ACKNOWLEDGMENTS
M. Asif appreciates the support of the Deanship of Scientific Research at the King Saud University for the Prolific Research Group PRG-1437-31.

References

1. P. Kouvaris, A. Delimitis, V. Zaspalis, D. Papadopoulos, S.A. Tsipas, N. Michailidis, *Mater. Lett.* 76 (2012)18-20.
2. J. Phillips, W. Bowen, E. Cagin, W. Wang, *Mater. Sci. Mater. Eng.* 6 (2011) 101-127.
3. V.V. Guliants, N.R. Shiju, *Appl Catal A Gen.* 356 (2009)1-17.
4. Y. Ju-Nam, J.R. Lead, *Sci Total Environ.* 400 (2008) 396-414.
5. W. Kim, K. Kim, B. Jung, J. Kim, *Sol Energy Mater Sol Cells*. 94 (2010) 1835-1839.
6. H.H. Park, Y.J. Choi, *Thin Solid Films.* 519 (2011) 6214-6218.
7. P. Quaresma, L. Soares, L. Contar, A. Miranda, I. Osorio, P.A. Carvalho, R. Franco, E. Pereira, *Green Chem.* 11 (2009) 1889-1893.
8. N. Tsibakhashvil, T. Kalabegishvili, V. Gabunia, E. Gintury, N. Kuchava, N. Bagdavadze, D. Pataraya, M. Gurielidzse, D. Gvarjaladze, L. Lomidze, *Nano Studies.* 2 (2010) 179-182.
9. S. Ananda Babu, S. Gurumallesh Prabu, *Mater. Lett.* 65 (2011)1675-1677.
10. M. Govarthanan, T. Selvankumar, K. Manoharan, (2014). *Int. J. Nanomed.* 9 (2014)1593-1599.
11. B. Nair, T. Pradeep, *Cryst Growth Des.* 2 (2002) 293-298.
12. S.V. Otari, R.M. Patil, N.H. Nadaf, S.J. Ghosh, S.H. Pawar, *Mater. Lett.* 72 (2012) 92-94.
13. S. Schultz, D.R. Smith, J.J. Mock, D.A. Schultz, Proceedings of the national academy of sciences, USA. 97(3) (2000) 996-1001.
14. J.S. Valli, B. Vaseeharan, *Mater. Lett.* 82, (2012) 171-173.
15. M.F. Zayed, W.H. Eisa, A.A. Shabaka, *Spectrochim Acta A* 98 (2012) 423-428.
16. A. Sengottaiyan, R. Mythili, T. Selvankumar, A. Aravinthan, S. Kamala-Kannan, K. Manoharan, P. Thiyagarajan, M. Govarthanan, J.H. Kim, *Res. Chem. Intermed.* 42 (2016) 3095-3103.
17. S. Ahmed, Saifullah, M. Ahmad, Babu Lal Swami, S. Ikram, J. Radiat. *Res. Appl. Sci.* 9 (2016) 1-7.
18. V. Kathiravan, S. Ravi, S. Ashok Kumar, S. Velmurugan, K. Elumalai, K. Chandra Prasad, *Spectrochim Acta A.* 139 (2015) 200-205.
19. M. J. Ahmed, G. Murtaza, A. Mehmood, T. M. Bhatti, *Mater. Lett.* 153 (2015) 10-13.
20. R. Samuel Akash Raj, S. Divya, S. Sindhu, K. Kasinathan, P. Arumugam, *Int. J. Pharm. Sci.* 6 (2014) 453-455.
21. T. C. Prathna, N. Chandrasekaran, A.M. Raichur, A. Mukherjee, *Colloids Surf. B.* 82 (2011)152-159.
22. Z. A. Ali, R. Yahya, S. D. Sekaran, R. Puteh, *Advan. Mater. Sci. Eng.* 2016 (2016) 1-6.
23. M. Satishkumar, K. Sneha, S. Won, C. W. Cho, S. Kim, Y.S. Yun, *Colloids Surf. B.* 73 332-338.
24. A. Bankar, B. Joshi, A.R. Kumar, S. Zinjarde, *Colloids Surf. A.* 368 (2010) 58-63.
25. A. Aravinthan, M. Govarthanan, K. Selvam, L. Praburaman, T. Selvankumar, R. Balamurugan, *Int. J. Nanomed.* 10, (2015) 1977-1983.
26. T. Y. Sumana, S. R. Radhika Rajasree, A. Kanchanab, S. Beena Elizabeth, Colloids Surf. B. 106 (2013) 74-78.
27. S. Dinesh, S. Karthikeyan, P. Arumugam, *Arch. Appl. Sci. Res.* 4 (2012) 178-187.
28. N. K. Monda, A. Chowdhury, U. Dey, P. Mukhopadhya, S. Chatterjee, K. Das, J.K. Datta, *Asian. Pac. J. Trop. Dis*. 4 (2014) S204-S210.
29. A.M. Hussein, *J. Saudi. Chem. Soc.* 14 (2010) 61-68.
30. G. Singhal, R. Bhavesh, K. Kasariya, A.R. Sharma, R.P. Singh, *J. Nanopart. Res.* 13 (2011) 2981-2988.
31. G.F. Fuhrmann, A. Rothstein, *Biochim Biophys Acta* 163 (1968) 331-338.
32. R.C. Murdock, L. Braydich-Stolle, A.M. Schrand, J.J. Schlager, S.M. Hussain, *Toxicol. Sci.* 101 (2008) 239-253.
33. K. Kalimuthu, R.S. Babu, D. Venkataraman, M. Bilal, S. Gurunathan, *Colloids Surf. B.* 65 (2008) 150-153.

34. B.D. Cullity, S.R. Stock, Elements of X-Ray Diffraction, 3rd Ed., Prentice-Hall Inc. (2001) p 167-171
35. A. Panacek, L. Kvitek, R. Prucek, K. Kolar, R. Vecerova, N. Pizurova, V.K. Sharma, T. Nevecna, R. Zbori, *J. Phys. Chem. B.* 110 (2006) 16248-16253.
36. M. Danilcauk, A. Lund, J. Saldo, H. Yamada, J. Michalik, *Spectrochim Acta A.* 63 (2006) 189-191.
37. A. Prabhu, K. Shankar, P. Muthukrishnan, A. Kathiresan, *J. Adv. Chem. Sci.* 2(3) (2016) 302–304.
38. J. Ren, L. Li, M. Cui, M. Zhai, C. Yu, X. Ji, Ionics, (2016) 1-9. doi:10.1007/s11581-016-1713-2
39. S. Mohan, F. Okumu, O. Oluwafemi, M. Matoetoe, O. Arotiba, *Int. J. Electrochem. Sci*. 11 (2016) 745-753.
40. Y. Song, K. Ma, F. Zhu, Z. Cheng, Y. Song, B. Dai1, J. Xu, *Int. J. Electrochem. Sci.* 8 (2013) 3628 3635.
41. Z. Yang, C. Qi, X. Zheng, J. Zheng, *Microchim Acta.* 183 (2016) 1131-1136.
42. S. Reddy, B.E. Kumara Swamy, H. Jayadevappa, *Electrochim. Acta*. 61 (2012) 78-86.
43. G. Pan, J. Chen, J. Guang, *Int. J. Electrochem. Sci*. 11 (2016) 5952-5961.
44. S. Reddy, R. Du, H. Xu, J. Wu, N. Mao, and J. Zhang, *Anal. Bioanal. Electrochem*. 7 (3) (2015) 277-290.
45. D. Huang, C. Chen, Y. Wu, H. Zhang, L. Sheng, H. Xu, Z. Liu, *Int. J. Electrochem. Sci.* 7 (2012) 5510 – 5520.
46. Y. Li, X. Lin, *Sensor. Actuat. B,* 115 (2006) 134–139.
47. F. Li, Y. Chai, R. Yuan, X. Li, Y. Yang, *J. Chin. Chem. Soc.* 62 (2015) 739-746.
48. A. Naseri, M.R. Majidi, *Daru.* 19 (2011) 270-276.
49. D. Zheng, J. Ye, L. Zhou, Y. Zhang, C. Yu, *J. Electroanal. Chem* 625 (2009) 82–87.
50. R. Zhang, J.G. Di, D. Chen, X.Y. Hu, *Sensor. Actuat. B,* 138 (2009) 174–181.
51. Y.R. Kim, S. Bong, Y.J. Kang, Y. Yang, R.K. Mahajan, J.S. Kim, H. Kim, *Biosens Bioelectron*. 25 (2010) 2366–2369.
52. A.A. Ensafi, M. Taei and T. Khayamian. *J. Electroanal. Chem*. 633 (2009) 212–220.
53. Y. Wang, W. Peng, L. Liu, M. Tang, F. Gao, M. Li, *Microchim Acta* 174 (2011) 41–46.
54. M. Noroozifar, M. Khorasani-Motlagh, R. Akbari, M.B. Parizi, *Biosens. Bioelectron*. 28 (2011) 56–63.
55. P.C. Pandey, D.S. Chauhan, V. Singh, *Electrochim Acta,* 54 (2009) 2266–2270.
56. Z.A. Alothman, N. Bukhari, S.M. Wabaidur, S. Haider. *Sens. Actuator B*, 146 (2010) 314–320.
57. C. Wang, J. Li, K. Shi, Q. Wang, X. Zhao, Z. Xionga, X. Zou, Y. Wang, *J. Electroanal Chem.* 770 (2016) 56–61.
58. X.H. Zhu, Y. Liang, X.X. Zuo, R.P. Hu, X. Xiao, J. Nan, *Electrochim. Acta*. 143 (2014) 366–373.